Modeling of Microwave Emission From Seasonally Frozen Ground Using Dense Media Radiative Transfer Theory (DMRT)

Jian Wang, Lingmei Jiang, *Member, IEEE*, Tianjie Zhao, *Senior Member, IEEE*, Huizhen Cui, *Member, IEEE*, and Yinghong Luan

***Abstract*— The freeze/thaw (F/T) transition of soil significantly affects water, energy, and carbon cycles at the land-atmosphere interface. The volumetric structure and vertical heterogeneity within the soil become apparent after soil freezing. This complicates the microwave radiative transfer process of frozen soil at different frequencies. In this study, a radiation transfer model, called SFS_DMRT, considering the volume scattering effects of seasonally frozen soil, is proposed based on dense media radiative transfer (DMRT) theory and the Mie spherical scattering model. The multiple scattering among discrete frozen soil clods is considered. This newly developed SFS_DMRT model is validated against ground radiometer measurements and compared with the advanced integral equation model (AIEM), a surface-scattering model, at three different experimental sites. Results show that in Sodankylä, where the soil is in a stable frozen state, the brightness temperature (Tb) simulated by SFS_DMRT has a higher agreement with observed Tb than that of AIEM. The emission of frozen soil is, moreover, better described by AIEM when the soil is undergoing diurnal F/T cycles in A'rou, in which the soil may freeze overnight and then thaw the next day. The Tb dependence on frequency was further examined, and results show that when simulating the passive microwave signature from the soil in a stable frozen state, which means the soil does not undergo intraday or diurnal F/T cycles, volume scattering effects can be ignored at the L-band; it should, however, be taken into consideration at Ku- and Ka-bands. The degree of volume scattering effects at C- and X-bands depends on the effective grain size of soil clods. The soil frost depth and microwave band penetration depth influence the attenuation of emissions from deeper unfrozen soil. The SFS_DMRT model developed in this study is vital for understanding the passive microwave signatures from frozen soil and can be used to obtain stratified profile information in layered soil.**

***Index Terms*— Frozen soil, L- to Ka-band, layered soil emission model, multiple scattering.**

Received 8 April 2024; revised 30 July 2024 and 14 September 2024; accepted 24 October 2024. Date of publication 5 November 2024; date of current version 14 November 2024. This work was supported by the National Key Research and Development Program of China under Grant 2021YFB3900104. *(Corresponding author: Lingmei Jiang.)*

Jian Wang is with the Research Institute of Forest Resource Information Techniques, Chinese Academy of Forestry, Key Laboratory of Forestry Remote Sensing and Information System, NFGA, Beijing 100091, China, and also with the Faculty of Geographical Science, Beijing Normal University, Beijing 100875, China (e-mail: wangjian@ifrit.ac.cn).

Lingmei Jiang is with the State Key Laboratory of Remote Sensing Science, Jointly Sponsored by Beijing Normal University and Aerospace Information Research Institute of Chinese Academy of Sciences, Faculty of Geographical Science, Beijing Normal University, Beijing 100875, China (e-mail: jiang@bnu.edu.cn).

Tianjie Zhao is with the State Key Laboratory of Remote Sensing Science, Aerospace Information Research Institute, Chinese Academy of Sciences, Beijing 100094, China (e-mail: zhaotj@aircas.ac.cn).

Huizhen Cui is with the National Space Science Center, Chinese Academy of Sciences, Beijing 100190, China (e-mail: cuihuizhen@nssc.ac.cn).

Yinghong Luan is with Shanghai Aerospace Electronic Technology Institute, Shanghai 201109, China (e-mail: lyhong0613@hotmail.com).

Digital Object Identifier 10.1109/TGRS.2024.3491861

I. Introduction

THE land surface freeze/thaw (F/T) transition restrains the terrestrial water cycle, climate change and carbon emissions from permafrost [1], [2], [3], [4], [5]. Frozen soil is characterized by a lower permittivity and significant volume scattering compared with thawed soil at microwave frequencies. Microwave remote sensing is well suited for land surface F/T monitoring and numerous studies have been conducted [6], [7], [8], [9].

The high contrast in permittivity between liquid water and ice leads to an obvious signal difference between frozen and thawed soil, which is the physical basis of F/T discriminant algorithms at microwave frequencies [10], [11], [12], [13], especially at L-band. High frequency (i.e., Ka-band) has also been proven useful in identifying land surface F/T status due to its sensitivity to land surface temperature [6], [14]. Meanwhile, previous studies have developed F/T classification algorithms based on the volume scattering effect of frozen soil, in which the negative spectral gradient between the Ku- and Ka-bands was observed and used to distinguish frozen soil [15], [16], [17]. The evaluation of those F/T classification algorithms showed that F/T results from the L-band show higher consistency with in situ 5 cm soil temperature compared with those from the Ka-band [18]. The F/T classification agreement between the L-band and Ka-band varies across forested and sparse vegetation [19]. Different frequencies have different sensitivities to the F/T process due to their respective penetration depths. Some studies revealed that the changing permittivity of the surface soil (∼2.5 cm) caused by diurnal F/T transitions dominated L-band brightness temperature (Tb) [13], [20], [21], [22], [23]. Other studies have presented that L-band Tb measurements do not reach their saturation up to a frost depth of 30 cm [10], [24].

Those studies, however, mainly focus on L-band, and the sensitivity of different frequencies to frozen soil parameters is not clear. Most of the models used to simulate microwave

signals from frozen soil, moreover, only consider surface scattering as a half-space medium [23], [24], [25]. The low liquid water content in frozen soil or dry soil leads to low soil dielectric constant. The optical thickness of frozen or dry soils arises due to the low imaginary part of the dielectric constant, causing a significant volume scattering effect [26]. The SMAP [7] and AMSR2 [8] F/T detection algorithms tend to incorrectly identify dry-thawed soil as frozen in arid and semi-arid climate regions [18]. That may be induced by the neglect of the volume scattering effect on passive microwave emissions. AMSR2 F/T detection algorithm considers soil as a surface scattering medium and ignores the volume scattering effect, which most likely exists in dry-thawed soil and frozen soil. The Normalized Polarization Ratio (NPR, SMAP F/T detector) of dry-thawed soil is low and close to the value of NPR of frozen soil due to low soil moisture (permittivity) and potential volume scattering in dry soil. Clarifying the sensitivities of microwave bands to the volume scattering effect of frozen soil is helpful for further understanding of the mechanism of monitoring soil F/T at different bands. The volume scattering effect of frozen soil on passive microwave signatures at different bands is, however, not clear at the current stage.

Several models, considering the volume scattering effect, have been developed for simulating the microwave signal of soil. The volume multiple scattering effects of dry sand were found by a ground-based passive microwave radiometer and simulated by a dense media radiative transfer (DMRT) model at C-, X-, Ku-, and Ka-bands [27]. For assessment of the influence of the soil volumetric structure on radar measurements, a 2-D numerical model was developed and evaluated with X-band radar backscattering coefficients, where dry soil was described as a mixture of fine earth and clods represented by randomly deformed ellipses [28]. By considering the volume multiple scattering of dry sand, the simulation Tb can obtain a better agreement with the ground-based observed Tb [27]. Frozen soil is similar to dry soil in that they are both mediums that have low soil moisture content compared to wet soil and are more transparent at the microwave band. In order to explain the negative spectral gradient between X-band and Ka-band from frozen soil, the first-order radiative transfer model and multiple scattering theory of frozen soil were used to analyze the relationship between Tb and scattering albedo at Ka-band [26]. A two-layer scattering model which consider the volume scattering effects was developed for simulating the radar backscattering coefficient and validated with numerical models at L- and P-bands [29]. This two-layer scattering model is a one-order scattering model that treats scatterers in frozen soil as ellipsoids and was originally used to describe the volume scattering of snow. In the two models for simulating frozen soil mentioned above, England et al. [26] used a simple empirical formulation to describe the single scattering effect at Ka-band. The application and validation of this model by [30] found that the simulated Tb at Ka-band vertical polarization (V- polarization) are closer to the ground-based measured Tb after considering the volume single scattering, but the consideration seemed insufficient. Du et al. [29] also analyzed the single scattering effect of frozen soil at low frequencies. Frozen soil is not as transparent as snow at the microwave band. The optical thickness of frozen soil can be large with low soil temperatures, which causes significant volume multiple scattering. Fung [31] also noted that the volume multiple scattering caused by discrete scatterers cannot be ignored at high frequency bands.

To describe the volume multiple scattering effects of frozen soil, the DMRT model was used to simulate the emission from frozen soil and validated with ground-based radiometric data [32]. Wang et al. [32], however, did not consider the boundaries' roughness; moreover, the model proposed in [32] was not fully validated against ground-based microwave radiometric data. Soil surface roughness has been proven to have a great effect on total emission simulation for a layered medium, such as the snowpack layer [33]. It is still not clear how the volume multiple scattering effect of frozen soil with a rough surface varies across different frequencies and stages of the freezing process.

Considering that the volume scattering effects of frozen soil would affect F/T classification accuracy, a radiative transfer model considering the volume multiple scattering effects of frozen soil based on DMRT was developed in order to improve the accuracy of F/T classification algorithms that are based on mechanism model and to provide theoretical model support for new satellite missions [i.e., China-French Water Cycle Observatory (CFWSAT) and Copernicus Imaging Microwave Radiometer (CIMR)]. In this model, the seasonally frozen soil was considered as a vertical heterostructure with frozen layer at the top and an unfrozen layer at the bottom, and the interfaces of unfrozen-frozen soil and frozen air were considered as rough surfaces. The ideal soil structure was mainly granular and approximately spherical, with a diameter of 0.25–10 mm [34]. The multiple scattering effects among frozen soil clods were considered with the DMRT model [35], where frozen soil clods were assumed to be spherical particles in this work. The spherical scattering phase matrix was described using the Mie scattering model. The emission from the unfrozen-frozen soil interface at the bottom and the air-frozen soil interface at the top were simulated with a multifrequency-polarization surface emission (Qp) model [36]. The Tb at L- to Ka-bands were simulated and validated with three different ground-based microwave radiometric data.

This work is organized as follows. In Section II, the radiometric data and ground measurements are briefly described. In Section III, a detailed description of the developed emission model is presented. In Section IV, the assessment of the model and sensitivity analysis are discussed, followed by a conclusion in Section V.

II. Data

The ground-based microwave radiometric data and soil parameters used in this study were collected from three different field experiments (Fig. 1): 1) at the A'rou site [Fig. 1(b)], Qinghai Province, China, the soil was observed undergoing intraday F/T transition at high frequencies (18.7 and 36.5 GHz); 2) at the Yudaokou site [Fig. 1(c)] in Hebei Province, China, frozen soil was observed at low frequencies (1.4, 6.925, and 10.65 GHz); and 3) at the Sodankylä site

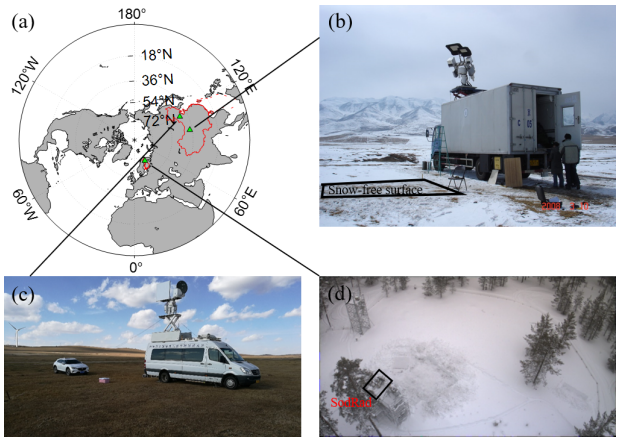

Fig. 1. (a) Locations of the three field experiments. (b) Microwave radiometer system at the A'rou site. (c) Microwave radiometer system at the Yudaokou site. (d) Microwave radiometer system at the Sodankylä site.

[Fig. 1(d)], Finland, frozen soil was observed at high frequencies (10.65, 18.7, and 36.5 GHz).

A. A'rou Experimental Site

The A'rou experimental site [Fig. 1(b)] is located in Qinghai Province, China (38.03°N, 100.43°E). It is a seasonally frozen ground and experiences frequent F/T cycles during the winter. A truck-mounted multifrequency microwave radiometer (TMMR) was used to measure Tb at the C-band (6.925 GHz), X-band (10.65 GHz), Ku-band (18.7 GHz) and Ka-band (36.5 GHz) with dual polarization on March 10 and 11, 2008, around the A'rou experimental site [25]; however, during this experiment, the receivers for the C- and X-bands were under repair. The Tb at Ku- and Ka-bands from the snow-free surface were observed at an incident angle of 50° every minute. Surface air and soil temperatures at 0–1, 1–4, and 4–7 cm depths were automatically measured with a data logger (Datataker, DT85) every minute. The soil moisture of the bottom unfrozen soil was measured using the weight method with a value of 0.2191 m^3/m^3. The in situ soil temperature and observed Tb are shown in Fig. 2(a). Soil temperatures at three depths were below 0 °C during the frozen period. The soil frost depth was set to 7 cm based on limited in situ soil temperature data due to a lack of frost depth measurements.

B. Yudaokou Experimental Site

The Yudaokou experimental site [Fig. 1(c)] is located in northern China (42.3868°N, 117.2186°E), which has a temperate and continental monsoon climate. It is also a seasonally frozen ground with a maximum frost depth of about 2 m. A six-channel dual-polarized microwave radiometer RPG-6CH-DP (Radiometer Physics GmbH, Germany) was fit in a van and used to measure surface emission in November 2016 [37]. The radiometer operated at L-band (1.4 GHz), C-band (6.925 GHz), and X-band (10.65 GHz) with dual polarization. The measured Tb values were available at incidence angles ranging from 30° to 60° with an interval of 5° every 10 or 20 min. Dual-polarized L-band channels at 40° and C- and X-band channels at 55° were used for this study. Soil moisture and temperature data at 3, 10, 20, 30, and 50 cm depths were automatically measured with Decagon's 5 TM sensors every 10 min. The observed data from November 9 to 12, when the soil emission was mainly affected by frozen soil rather than snow melting, were selected to verify the developed model. According to the in situ soil temperature data shown in Fig. 2(b), the soil frost depth was set to 10 cm. The temperature of the frozen soil was the mean temperature at depths of 3 and 10 cm. The soil moisture and temperature of unfrozen soil in the bottom layer were 0.35 m^3/m^3 and 274 K, respectively, as the average of the 30 and 50 cm measurements.

TABLE I
OBSERVED INFORMATION AT THE THREE EXPERIMENTAL SITES

Sites	Soil texture (clay, sand, %)	Bulk density (g/cm^3)	Bands	Soil frozen depth (cm)
A'rou	10.3, 28.66	0.83	Ku and Ka	7
Yudaokou	18, 60	1.0126	L, C and X	10
Sodankylä	1, 70	1.5761	X, Ku and Ka	80

C. Sodankylä Experimental Site

The Sodankylä experimental site [Fig. 1(d)], the intensive observation area (IOA), is located in northern Finland (67.3618°N, 26.6338°E) [38], and the soil is freezing seasonally. This site was located on a forest clearing surrounded by a sparse forest. The Tb at the X-band (10.65 GHz), Ku-band (18.7 GHz), and Ka-band (36.5 GHz) from the snow-removed surface were observed by a SodRad radiometer with dual polarization from March 3 to 15, 2016 at incidence angles ranging from 40° to 60°. The Tb at 50° was used in this study. The snow-free surface observed by SodRad was prepared by removing a thick snow layer (>50 cm), but there were still a few ice particles left. Soil moisture and temperature data at a 5 cm depth in eight different spots were automatically measured with Stevens Hydra Probe II. Among these eight spots, spot 1 to spot 4 were set in the snow-free observation area. The mean soil moisture of spots 1–4 measured from unfrozen soil in early November was used as the soil moisture of bottom unfrozen soil, which was 0.1227 m^3/m^3. The in situ soil temperature and observed Tb from the snow-free surface are shown in Fig. 2(c). The soil frost depth was obtained from frost tube measurements from the site (67.3392°N, 26.6265°E) near the radiometer observation area, which was 80 cm.

The soil parameters of the three experimental sites are given in Table I. The sand contents were high at the Yudaokou and Sodankylä sites, with values of 60% and 70%, respectively.

III. THEORETICAL MODELING DEVELOPMENT

In this study, the seasonally frozen soil is deemed as an irregular inhomogeneous layer shown in Fig. 3. The upper soils usually freeze during wintertime when the soil temperature is below 0 °C; therefore, the seasonally frozen soil profile is composed of a layer of frozen soil, stacked on top of a layer of unfrozen soil. In moist soils, freezing is the process by which the water in the soil changes from liquid to ice. We assume that the phase state of water is significant difference between the upper frozen soil and the unfrozen subsoil, which in upper frozen soil is primarily ice and in unfrozen subsoil

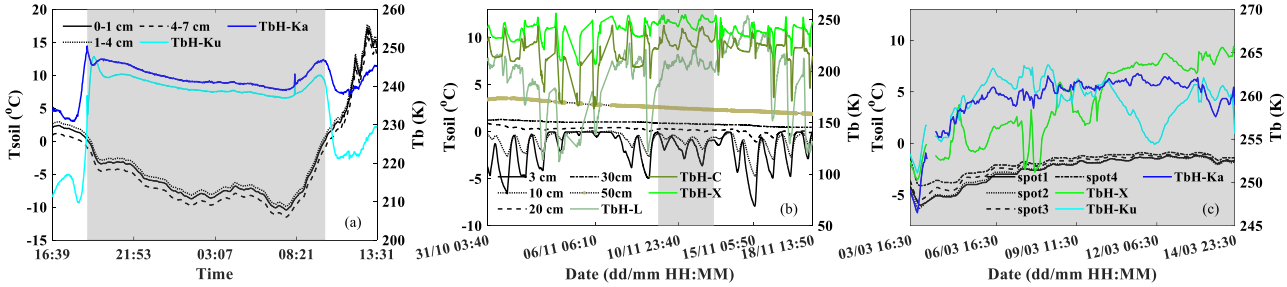

Fig. 2. Time series of measured soil temperature and Tb (at H-polarization, as an example) at (a) A'rou site, (b) Yudaokou site, and (c) Sodankylä site. The data in the gray shaded zone were measured from the frozen period and used to explore the volume scattering effect.

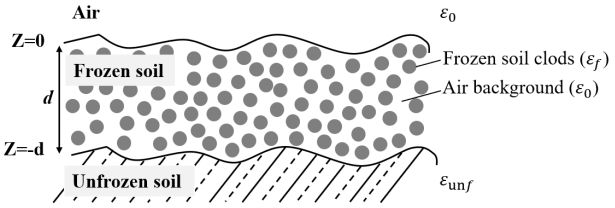

Fig. 3. Representation of the layered, seasonally frozen soil, including upper frozen soil and bottom unfrozen soil.

is primarily liquid water. Even if water redistribution occurs between the bottom unfrozen soil and the upper frozen soil layer [39], the warmer unfrozen subsoil has a higher liquid water content [40]. The decrease in liquid water content caused by soil freezing leads to a decrease in soil dielectric constant. The optical thickness of upper frozen soils arises due to the reduction of the imaginary part of the dielectric constant. As a result, the absorption of microwave signals by frozen soil is significantly reduced compared to the moist, unfrozen subsoil, which, in turn, leads to a nonnegligible volume scattering effect within frozen soil. In contrast, in moist, unfrozen subsoils, which are regarded as semi-infinite medium with infinite optical thickness, waves are only transmitted and not reflected. There is no need to consider volume scattering within unfrozen subsoils.

Since the effect of the upper frozen soil volume multiple scattering on passive microwave emission is nonnegligible. We consider a frozen soil layer as a volume of dense media consisting of spheres of soil clods suspended in an air background. As shown in Fig. 3, the frozen soil layer thickness is d. ε_f is the dielectric constant of the spherical frozen soil clods, ε_0 is the dielectric constant of the host (air), ε_{unf} is the dielectric constant of the bottom unfrozen soil, which is modeled as a semi-infinite medium. For volume scattering media, scatterers are randomly oriented and distributed, acting like spherical scatterers even if they are nonspherical [41]. An ideal soil structure is, moreover, mainly granular and approximately spherical, with a diameter of 0.25–10 mm [34]. In this study, therefore, frozen soil clods mainly consisting of soil particles, bound water that surrounds the mineral surfaces and remains unfrozen, and ice crystals were deemed as dominant scatterers and assumed to be spherical, and air is still assumed as the background medium, as with DMRT [35]. The spherical scattering phase matrix was described with the Mie scattering model. For considering the coherent effect, the pair distribution function of the dense media particle positions was defined by DMRT. A one-layer DMRT/quasicrystalline approximation (QCA) with the Mie scattering was used to simulate the Tb emissions from seasonally frozen soil (hereafter referred to as SFS_DMRT).

In order to describe the multiple scattering within the frozen soil layer, full multiple scattering effects with 16 Gaussian quadrature angles were considered, and microwave emission followed the DMRT theory. DMRT theory has proven useful in simulating multiple scattering effects within layered dry snow [35], [42] and dry sand [27]. The DMRT equations for passive remote sensing are as follows [35]:

$$\begin{aligned}
&\cos\theta \frac{d\bar{I}(\theta,\emptyset,z)}{d_z} \\
&= -\overline{\overline{k}}_e(\theta,\emptyset)\bar{I}(\theta,\emptyset,z) + k_a\overline{T} + \int_0^{\frac{\pi}{2}} d\theta' \sin\theta' \\
&\quad \times \int_0^{2\pi} d\emptyset' [\overline{\overline{P}}(\theta,\emptyset;\theta',\emptyset')\bar{I}(\theta',\emptyset',z) \\
&\qquad + \overline{\overline{P}}(\theta,\emptyset;\pi-\theta',\emptyset')\bar{I}(\pi-\theta',\emptyset',z)]
\end{aligned} \tag{1}$$

$$\begin{aligned}
&-\cos\theta \frac{d\bar{I}(\pi-\theta,\emptyset,z)}{d_z} \\
&= -\overline{\overline{k}}_e(\pi-\theta,\emptyset)\bar{I}(\pi-\theta,\emptyset,z) + k_a\overline{T} \\
&\quad + \int_0^{\frac{\pi}{2}} d\theta' \sin\theta' \int_0^{2\pi} d\emptyset' [\overline{\overline{P}}(\pi-\theta,\emptyset;\theta',\emptyset')\bar{I}(\theta',\emptyset',z) \\
&\qquad + \overline{\overline{P}}(\pi-\theta\emptyset;\pi-\theta'\emptyset')\bar{I}(\pi-\theta'\emptyset' z).
\end{aligned} \tag{2}$$

Here, $\bar{I}(\theta,\emptyset,z)$ is the specific intensity at Gaussian quadrature angle θ at vertical and horizontal polarizations in frozen soil layer. $\overline{\overline{P}}$ is the phase matrix of the discrete random medium, formed and calculated the same here as in [42, eq. (16)]. k_e and k_a are the extinction coefficient and absorption coefficient, respectively, and can be calculated by [42, eqs. (4) and (12)]. T is the thermodynamic temperature of the frozen soil layer.

The equations can be solved by matching boundary conditions as follows, and the corresponding details can be found in [35], [42], and [43].

$$\begin{aligned}
&\text{At } z = 0 \\
&\bar{I}_1(\pi-\theta,\emptyset,z=0) = \overline{\overline{R}}_{10}(\theta)\bar{I}_1(\theta,\emptyset,z=0) \\
&\text{At } z = -d \\
&\bar{I}_2(\theta,\emptyset,z=-d) = \overline{\overline{R}}_{12}(\theta)\bar{I}_2(\pi-\theta,\emptyset,z=-d) + \overline{\overline{T}}_{21}(\theta)T_2
\end{aligned} \tag{3, 4}$$

where $\overline{\overline{R}}_{10}$ and $\overline{\overline{R}}_{12}$ are the reflectivity matrix at the frozen soil–air and frozen soil–unfrozen soil boundary, respectively. $\overline{\overline{T}}_{21}$ is the transmissivity matrix from unfrozen soil to frozen soil. T_2 is the thermodynamic temperature of the unfrozen soil layer. The stickiness parameter was set at 0.1 for each layer based on [35]. Although the effect of multiple scattering within frozen soil is what we would like to focus on through the DMRT theory, the roughness at the boundaries should not be ignored [33], [44], [45], [46], especially for media with rough interfaces such as soil. In [35], the Q/H model [47] was used to account for the influence of roughness at the ground-snow interface. Qp model [36] was developed through an advanced integral equation model (AIEM) simulated database and was considered to have an accuracy close to that of AIEM in simulating rough surface emission. Qp model, moreover, performs better than Q/H model and gives higher accuracy for high-frequency [36]. In this study, therefore, the Qp model [36] is used to consider the surface roughness effects and calculate the surface effective reflectivity at unfrozen-frozen soil interface, and frozen soil-air interface. Then the transmissivity is calculated as one minus the surface effective reflectivity. As for the dielectric constant of soil scatterers, there are fewer studies on the dielectric constant of soil clods or scatterers. In previous studies on the volume scattering effects of dry soil [28], the clod had a relative permittivity of three at 10 GHz, which corresponds to very dry soil. As for frozen soil [29], soil clods were deemed as dominant scatterers, and the dielectric constant of the scatterers was set to 8.5 at L- and P-band. Similar to these studies, the dielectric constant of the scatterers was set to a fixed value in this study. Considering the differences in soils at different experimental sites, the dielectric constant of scatterers is, however, different from one experimental site to another and varies with frequency. Then, the effective dielectric constant of frozen soil is calculated as $\varepsilon_{\text{eff}} = (K_r/k)^2$ [42], where $K_r = Re(K)$, K is the effective propagation constant related to the dielectric constant of frozen soil scatterers, and k is wavenumber. The fractional volume (f_v) of the scatterers in upper frozen soil is another parameter to be determined. In this study, the aggregates of soil particles, bound water, and ice crystals were deemed as dominant scatterers, and air is assumed as the background medium. A unit volume of frozen soil is assumed as the sum of soil porosity and fractional volume of the scatterers. For unfrozen soil, soil porosity (f) is the volume fraction of soil pores to unit volume soil and can be expressed as follows:

$$f = 1 - \frac{\rho_b}{\rho_s} \tag{5}$$

ρ_b and ρ_s are the soil bulk density and soil particle density, respectively. Changes in soil porosity and soil volume after soil is frozen are complex. Assuming that the volume of the soil remains constant after being frozen, the increase in scatterer volume caused by the increase in ice leads to a smaller soil porosity. Studies have, however, pointed out that the freeze leads to an increase in soil volume, in addition to an increase in soil porosity [48]; that is, changes in soil porosity and soil volume after soil frozen are complex and difficult to estimate.

TABLE II
OPTIMAL PARAMETERS AT EACH EXPERIMENTAL SITE

	A'rou	Yudaokou	Sodankylä
Rms height (cm)	2.5	2.1	2.5
Correlation length(cm)	10	11	9
Effective frozen soil grain size (cm)	0.24	0.4	0.11

Here, we focus on the volume multiple scattering effects of frozen soil and do not explore the complex coupled changes in total volume and porosity of soil after frozen. We assume that soil porosity does not change before and after the soil is frozen. The fractional volume of scatterers is, therefore, defined as

$$f_v = 1 - f = \frac{\rho_b}{\rho_s}. \tag{6}$$

In summary, the input parameters of the SFS_DMRT model, i.e., the soil temperature, soil texture, soil bulk density, soil frost depth, and fractional volume of scatterers, can be obtained through field observations and model calculations. The effective frozen soil particle size and surface roughness (Root mean square height (rms height) and correlation length) were the fitting parameters since there were no direct measurements. In this study, some observation data with different frozen soil temperatures were selected to optimize the effective frozen soil particle size and surface roughness at each experimental site. First, AIEM was used to optimize the surface roughness at each experimental site. After obtaining the optimal surface roughness, the effective frozen soil particle size was optimized with the SFS_DMRT model. In the process of optimizing parameters, the errors between the simulated and observed Tb were calculated for all possible surface roughness or effective frozen soil particle sizes according to the following equation:

$$\text{error} = \frac{1}{3}\sum_{i=1}^{n}\left(\sigma^2_{\text{TbH}} + \sigma^2_{\text{TbV}} + \sigma^2_{\text{TbH-TbV}}\right) \tag{7}$$

where σ^2_{TbH}, σ^2_{TbV}, and $\sigma^2_{\text{TbH-TbV}}$ are the root mean square errors (RMSEs) of Tb at the H and V-polarizations and the difference between the H- and V-polarizations, respectively, n refers to the number of observation data. The optimal surface roughness or effective frozen soil particle size can be determined when the error is at its minimum. In this study, AIEM was used to simulate the surface scattering from frozen soil to facilitate a comparison with the SFS_DMRT model.

IV. RESULTS AND DISCUSSION

A. Comparison Between Experimental Data and Model Simulation

First, the surface roughness and effective frozen soil particle size were determined by the optimal iteration method and are shown in Table II. In this study, the unfrozen–frozen soil and frozen soil–air interfaces were assumed to have the same surface roughness. The effective frozen soil particle size was optimized with the observed data at the highest frequency at each experimental site since high frequencies are more sensitive to volume scattering effects.

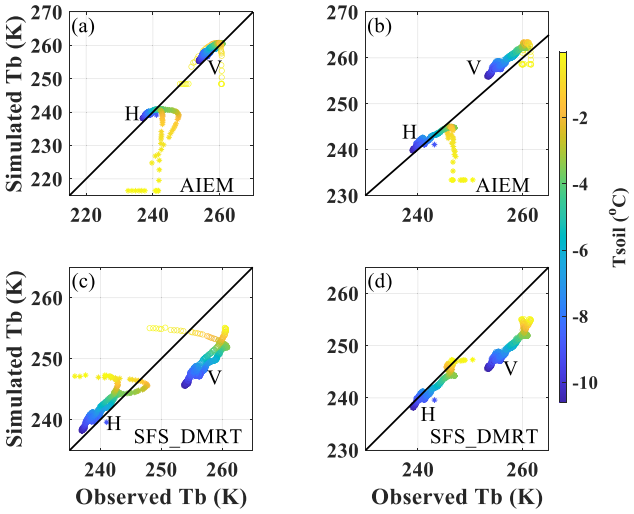

Fig. 4. Comparison of the simulated Tb using (a) and (b) AIEM and (c) and (d) SFS_DMRT with the observed Tb at the A'rou site: (a) and (c) 18.7 GHz and (b) and (d) 36.5 GHz.

TABLE III
ERROR STATISTICS FOR THE COMPARISON BETWEEN THE SIMULATED AND OBSERVED TB AT THE A'ROU SITE

	RMSE (K)		Bias (K)		Correlation coefficient	
	SFS_DMRT	AIEM	SFS_DMRT	AIEM	SFS_DMRT	AIEM
Tb18.7H	16.45	1.34	16.41	0.09	0.82	0.86
Tb18.7V	5.19	1.48	4.91	1.21	0.7	0.94
Tb36.5H	1.24	1.03	-0.99	0.21	0.96	0.95
Tb36.5V	7.72	2.71	-7.7	2.64	0.96	0.96

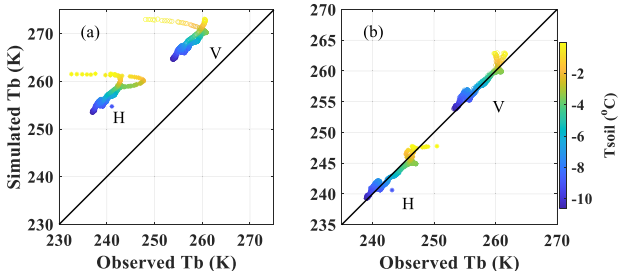

Fig. 5. Comparison of the simulated Tb using SFS_DMRT (transition layer was added) with the observed Tb at the A'rou site (a) 18.7 GHz and (b) 36.5 GHz.

Fig. 4 shows the comparison of the simulated Tb using AIEM and SFS_DMRT versus the observed Tb at the A'rou site. In SFS_DMRT, the dielectric constants of scatterers are 2.78 + 0.21 i at 18.7 GHz and 2.57 + 0.12 i at 36.5 GHz, respectively. The performance of both SFS_DMRT and AIEM were significantly degraded when soil temperature is above −3 °C, in which case the soil may have been undergoing an F/T transition and exhibit complex compositions. The complex soil composition and scattering mechanisms during this period may result in poor performance for both models. To assess the capability of SFS_DMRT to estimate frozen soil emissions, Table III shows the RMSE, bias, and correlation coefficient for both SFS_DMRT and AIEM based on observed Tb when soil temperature is below −3 °C. The RMSEs obtained from the AIEM results and SFS_DMRT results are in the range of 1.03–2.71 K and 1.24–16.45 K, respectively. The bias obtained from the AIEM results and SFS_DMRT results are in the range of 0.09–2.64 K and −0.99 to 16.41 K, respectively. In Fig. 4 and Table III, the results show that AIEM predicts emission behavior better at 18.7 and 36.5 GHz compared to SFS_DMRT. The smallest RMSE and bias were obtained with AIEM. Tb was overestimated at 18.7 GHz by SFS_DMRT. At the A'rou site [Fig. 1(c)], although the snow was removed, the volume scattering of the ice crust remaining on the soil surface also affected the observed Tb. The mixture of ice crust and air bubble layers covering the frozen soil as a homogeneous transition layer with a small thickness were modeled with DMRT [49]. The depth of the transition layer, density and grain radius of the ice crust were fit as 0.6 cm, 0.28 g/cm^3, and 0.2 cm, respectively. The measured air temperature was used as the temperature of this transition layer. Fig. 5 shows a comparison of the simulated Tb using SFS_DMRT with the transition layer covered with the observed Tb. After considering the transition layer, an improvement of the agreement between SFS_DMRT simulated Tb and observed Tb can be observed in Ka band. The RMSE of the Tb at Ka-band decreased to 0.82 and 0.8 K at the H- and V-polarizations, respectively. From Tables I and II, it can be seen that the sand content and effective frozen soil particle size were small at the A'rou site. Since the effect of the volume scattering of frozen soil at 18.7 GHz was smaller than that at 36.5 GHz, the optimal effective frozen soil particle size at 18.7 and 36.5 GHz might be different [41]. It was found that for 18.7 GHz, the SFS_DMRT simulated Tb is in high agreement with the observed Tb with a 0.5 cm frozen soil particle size. The effective frozen soil particle size optimized with 36.5 GHz led to an underestimation of the effect of volume scattering and an overestimation of the Tb at 18.7 GHz. This can also be attributed to the intraday F/T transition of soil, which was not in a stable frozen state. The frozen soil albedo calculated by SFS_DMRT at 18.7 and 36.5 GHz were 0.27 and 0.63, respectively. The relatively small albedo and unstable frozen state of the frozen soil indicate that the volume scattering effect of frozen soil on Ku-band might not be obvious at the A'rou site. The frozen soil emissions might be described by AIEM without considering the volume scattering effect at the A'rou site.

The observation frequencies of the ground-based microwave radiometric experiment at the Yudaokou experimental site are L-, C-, and X-band. Since the Qp model was developed based on the configuration of AMSR-E (no L-band), in order to demonstrate that it can be applied to the L-band, we first compared the L-band emissivity simulated by the Qp model with that simulated by the AIEM. The model parameters corresponding to different frequencies (i.e., C-, X-, Ku- and Ka-band) in the Qp model are different. We choose the model parameters of C-band, which is closest to the L-band, to calculate the L-band emissivity. The input soil parameters of Qp and AIEM models were referenced to the measured data from the Yudaokou experimental site, where soil moisture was 0.15 m^3/m^3, soil temperature was the mean temperature at depths of 3 and 10 cm, soil root mean square height was 1 cm, soil correlation length was 11 cm, soil sand content was 60%, soil clay content was 20%, and soil bulk density was 1.3 g/cm^3.

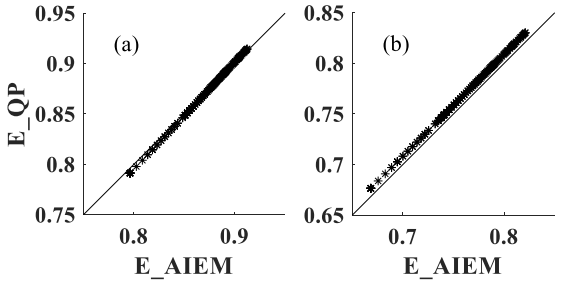

Fig. 6. Comparison of emissivity calculated by AIEM and Qp model (a) V-polarization and (b) H-polarization.

Fig. 6 shows the comparison of the L-band emissivity at an incidence angle of 40° calculated by the Qp model and the AIEM model, respectively. As can be seen in Fig. 6, there is almost no difference between the two models at vertical polarization, and only a very slight difference between the two bands at horizontal polarization. The Qp model was, therefore, used to calculate the L-band emissivity at the Yudaokou site.

Fig. 7 shows the comparison of the simulated Tb using AIEM and SFS_DMRT versus the observed Tb at the Yudaokou site. The dielectric constants of scatterers are 7.17 + 0.66 i at 1.41 GHz, 5.75 + 0.11 i at 6.925 GHz and, 4.53 + 0.93 i at 10.65 GHz respectively. Table IV presents the RMSE, bias, and correlation coefficient of both SFS_DMRT and AIEM based on the observed Tb at the Yudaokou site. The RMSEs obtained from the AIEM results and SFS_DMRT results are in the range of 3.73–39.43 K and 4.26–22.56 K, respectively. The bias obtained from the AIEM results and SFS_DMRT results are in the range from −38.65 to 2.13 K and from −22.28 to 17.12 K, respectively. From Fig. 7 and Table IV, it can be seen that using AIEM for simulating frozen soil emissions at 1.4 GHz and V-polarization at 6.925 and 10.65 GHz contributed to the lowest RMSE and bias and the highest correlation coefficient. A negative bias for the H-polarization at 6.925 and 10.65 GHz can be observed using AIEM, which was solved by SFS_DMRT. SFS_DMRT reduced the RMSE from 28.8 to 18.5 K at 6.925 GHz H-polarization and from 39.34 to 4.26 K at 10.65 GHz H-polarization. The simulation errors for H-polarization at 6.925 and 10.65 GHz using AIEM were reduced by considering the volume scattering effect. As seen in Fig. 7(d)–(f), the Tb calculated by SFS_DMRT, however, had a small numerical range and great polarization difference, which is quite different from the observed Tb. It can be seen from Fig. 7 that when soil temperature changes within the range of 3 K, the observed Tb changes reach 20 K. Meanwhile, the Tb simulated by SFS_DMRT ranges within 10 K. In situ air temperature data at the Yudaokou experimental site range from 252 to 272 K and reached 20 K, which may lead to the fluctuation of surface soil moisture. Fluctuating air temperature and surface soil moisture may dominate the large changes in observed Tb. Soil moisture in unfrozen soil and dielectric constants of scatterers were, however, set as constant values in models, which may lead to a small variation of Tb simulated by SFS_DMRT. This shows that the SFS_DMRT model is not effective in simulating the passive microwave Tb of frozen soil with a negative temperature but close to 0 °C.

TABLE IV
ERROR STATISTICS FOR THE COMPARISON BETWEEN THE SIMULATED AND OBSERVED TB AT THE YUDAOKOU SITE

	RMSE (K)		Bias (K)		Correlation coefficient	
	SFS_DMRT	AIEM	SFS_DMRT	AIEM	SFS_DMRT	AIEM
Tb1.4H	10.18	8.25	-5.99	0.27	-0.47	0.57
Tb1.4V	22.56	7.32	-22.28	-0.57	-0.34	0.18
Tb6.925H	18.25	28.8	17.12	-27.98	-0.22	0.62
Tb6.925V	14.91	4.45	14.74	2.13	-0.2	0.51
Tb10.65H	4.26	39.34	1.77	-38.65	0.07	0.29
Tb10.65V	11.4	3.73	11.13	1.99	-0.17	0.45

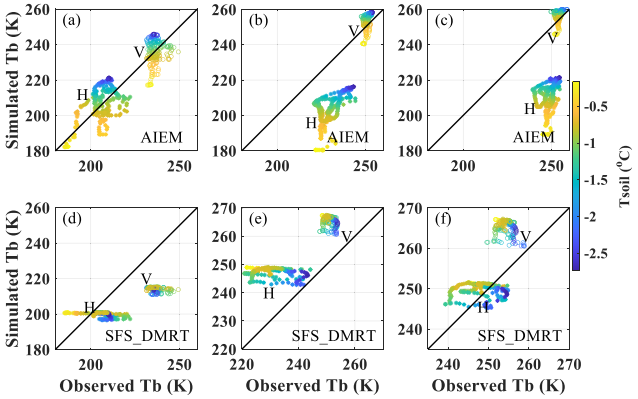

Fig. 7. Comparison of the simulated Tb using (a)–(c) AIEM and (d)–(f) SFS_DMRT with the observed Tb at the Yudaokou site: (a) and (d) 1.4 GHz, (b) and (e) 6.925 GHz, and (c) and (f) 10.65 GHz.

The frozen soil albedo calculated by SFS_DMRT in Fig. 6(d)–(f) at 1.4, 6.925, and 10.65 GHz are 0.003, 0.08 and 0.13, respectively. The albedo indicates that volume multiple scattering in frozen soil could be ignored at low frequencies (i.e., L-band); therefore, the Tb calculated by SFS_DMRT could be close to the Tb calculated by AIME at L-band under certain conditions. As shown in Fig. 7, the Tb values calculated by AIEM and SFS_DMRT were, however, different. SFS_DMRT treated soil as a two-layer structure. The soil frost depth and emissivity from the bottom unfrozen soil influenced the results from SFS_DMRT at L-band, which has deep penetration depth. To analyze the influence of soil frost depth, the Tb at L-band was calculated using SFS_DMRT with a soil frost depth from 1 to 200 cm in 10 cm-step increments and compared it with the Tb calculated using AIEM, as shown in Fig. 8. For SFS_DMRT, the emission from the bottom unfrozen soil was fixed and lower than that from the frozen soil due to the fixed soil parameters and large soil moisture (0.35 m^3/m^3 as described in the Data section). Fig. 8 shows the scatter plot of the Tb between AIEM and SFS_DMRT with the frozen soil temperature range from 243 to 263 K and soil frost depth range from 1 to 200 cm. The soil frost depth at Yudaokou is about 10 cm. As seen in Fig. 8, when the frost depth was approximately 10 cm, the Tb simulated by SFS_DMRT was significantly lower than that of the AIEM. This is most likely because the emissivity from the bottom unfrozen soil contributed greatly to the total emissivity of the soil in the case where the thickness of the upper frozen layer is 10 cm. The simulation of SFS_DMRT is close to that of AIEM when the soil frost depth is about 50 cm.

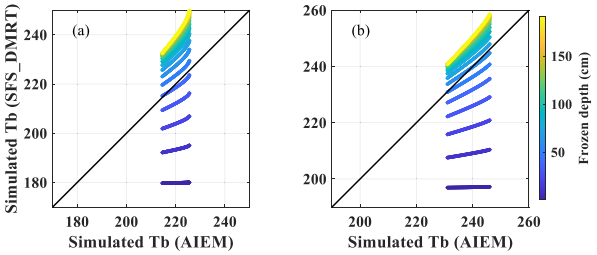

Fig. 8. Scatter plot of the Tb simulated by AIEM and SFS_DMRT with the frozen soil temperature range from 243 to 263 K and soil frost depth range from 1 to 200 cm. The color bar represents the soil frost depth. (a) H-polarization and (b) V-polarization.

In summary, the results indicate that the effect of the volume scattering of frozen soil might be negligible at the L-band or even C-band at the Yudaokou site, probably because the surface scattering strength is high enough relative to volume scattering in frozen soil layer at low frequencies (i.e., L- and C-band). The soil frost depth is one of the determining factors of the influence of the emissivity from bottom unfrozen soil on the Tb calculated by SFS_DMRT. The SFS_DMRT model is not suitable when frozen soil has negative temperatures but is close to 0 °C.

Fig. 9 shows the comparison of the simulated Tb using AIEM and SFS_DMRT versus the observed Tb at the Sodankylä site, respectively. The dielectric constants of scatterers are 3.6 + 0.06 i at 10.65 GHz, 3.5 + 0.0.05 i at 18.7 GHz, and 3.4 + 0.03 i at 36.5 GHz, respectively. Different from the previous two experimental sites, the soil was totally frozen at the Sodankylä site with a depth of 80 cm. From Fig. 9(a)–(c), the simulated Tb was obviously underestimated by AIEM, and the polarization difference at the three frequencies was greater than that from the observed Tb. The simulation results were significantly improved in Fig. 9(d)–(f) by considering the volume scattering effect. The Tb at H-polarization was close to the observed Tb at the three frequencies; however, the polarization difference at the three frequencies was still obvious compared with the observed polarization difference. The small polarization separation shown in the observed Tb could be due to the volume scattering from a thin layer of ice covering the frozen soil [41], [50]. At the Sodankylä site, although the snow was removed, ice crust remained on the soil surface, and the volume scattering of this ice crust also affected the observed Tb. The mixture of the ice crust and air bubble layers covering the frozen soil were modeled as a homogeneous transition layer with a small thickness with DMRT [49]. The transition layer depth, density and grain radius of the ice crust were fit as 0.1 cm, 0.13 g/cm^3, and 0.06 cm, respectively. The measured air temperature was used as the temperature of this transition layer. Fig. 10 shows the comparison between the SFS_DMRT simulated Tb and observed Tb when the soil surface was covered by the transition layer. The simulated Tb with the transition layer was much closer to the observed Tb than those from AIEM as a surface-scattering model and from SFS_DMRT without considering the transition layer. Table V shows the RMSEs, biases, and correlation coefficients of AIEM, SFS_DMRT, and SFS_DMRT, considering the transition layer based on the observed Tb at the Sodankylä site. The RMSEs obtained from the AIEM results, SFS_DMRT results, and SFS_DMRT with the transition layer results are in the range of 6.75–26.34 K, 1.2–8.68 K, and 0.96–3.02 K, respectively. The bias obtained from the AIEM results, SFS_DMRT results, and SFS_DMRT with the transition layer results are in the range from −26.11 K to −6.52, from −8.41 to −0.33 K, and from −2.12 to 2.04 K, respectively. The smallest RMSE and bias were obtained by SFS_DMRT considering the transition layer. The low correlation coefficient between the observed Tb and the simulated Tb from SFS_DMRT with the transition layer is due to the large Tb difference at soil temperature around −1 °C.

The scattering albedo in the frozen soil layer calculated by SFS_DMRT in Fig. 10 at 10.65, 18.7, and 36.5 GHz are 0.003, 0.02 and 0.17, respectively. The effect of the volume scattering of a thin transition layer could narrow the polarization difference and improve the simulations. The results from the Sodankylä site demonstrate that it is necessary to consider the effect of volume scattering of soil in a stable frozen state, especially at high frequencies.

TABLE V

ERROR STATISTICS FOR THE COMPARISON BETWEEN THE SIMULATED AND OBSERVED TB AT THE SODANKYLÄ SITE

	RMSE (K)			Bias (K)			Correlation coefficient		
	AIEM	SFS_DMRT	Transition layer	AIEM	SFS_DMRT	Transition layer	AIEM	SFS_DMRT	Transition layer
Tb10.65H	26.34	6.86	3.02	-26.11	-5.76	2.04	0.8	0.8	0.58
Tb10.65V	10.45	1.73	0.96	-10.4	-1.27	0.22	0.96	0.96	0.95
Tb18.7H	24.68	5.99	2	-24.6	-5.43	-1.57	0.36	0.36	0.92
Tb18.7V	8.66	1.2	1.47	-8.59	-0.33	1.13	0.93	0.93	0.95
Tb36.5H	23.83	8.68	2.78	-23.77	-8.41	-2.12	0.81	0.81	0.8
Tb36.5V	6.75	2.33	2.49	-6.52	-1.51	1.88	0.87	0.87	0.82

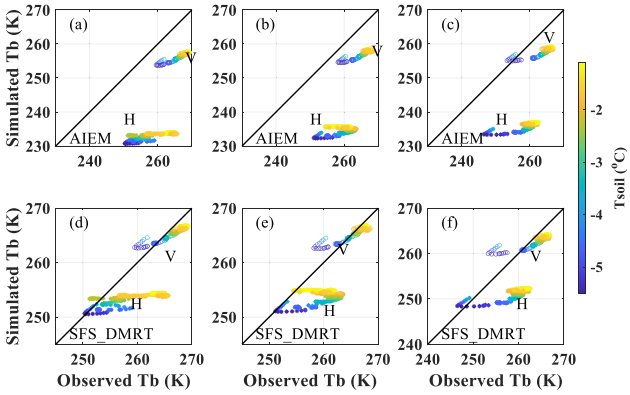

Fig. 9. Comparison of the simulated Tb using AIEM (a)–(c) and SFS_DMRT (d)–(f) with the observed Tb at the Sodankylä site (a) and (d) 10.65 GHz, (b) and (e) 18.7 GHz and (c) and (f) 36.5 GHz.

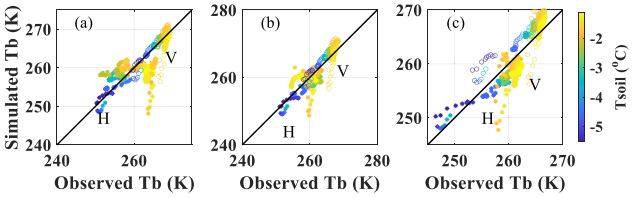

Fig. 10. Comparison of the simulated Tb using SFS_DMRT (transition layer was added) with the observed Tb at the Sodankylä site. (a) 10.65 GHz, (b) 18.7 GHz, and (c) 36.5 GHz.

B. Effects of Frozen Soil Parameters on Tb

Based on the evaluation of simulated Tb using SFS_DMRT, it was found the following three main frozen soil parameters influencing SFS_DMRT simulation results, including: 1) effective frozen soil particle size, 2) soil frost depth, and 3) dielectric constants of scatterers. In this section, the sensitivity of the above three parameters to the Tb simulated by SFS_DMRT were analyzed. Soil temperature at the lower half-space (unfrozen soil) was set at 5 °C, while the temperature of frozen soil at the top layer was set to −15 °C, which could indicate a stable frozen state. We focused on analyzing the influences of the frozen soil parameters on the simulations and set the surface as a relatively smooth surface (rms height = 1 cm, correlation length = 10 cm). The observation angles were 40° at L-band (similar to the SMAP mission) and 55° at C- to Ka-bands (similar to the AMSR-E/2 sensors).

C. Effective Frozen Soil Particle Size on Tb Simulation

The DMRT/QCA was developed for moderate-size particles [51]. Considering the penetration of different bands into frozen soil particles, we simulated Tb from L- to Ka-band with the effective frozen soil particle diameter ranging from 0.05 cm to approximately 0.4 of the wavelength of each band with a step size of 0.01 cm. The maximum effective particle size of frozen soil particles was set as 1 cm because an ideal soil structure is approximately spherical with a maximum diameter of 1 cm [34]. The soil frost depth and soil moisture of the unfrozen soil layer were 10 cm and 0.15 m^3/m^3, respectively. The dielectric constants of scatterers are 4.4 + 0.17 i at L-band, 3.7 + 0.23 i at C-band, 3.5 + 0.2 i at X-band, 3.2 + 0.13 i at Ku-band and 3.1 + 0.07 i at Ka-band, respectively. The sand content, clay content, and bulk density of the soil were 60%, 20%, and 1.3 g/cm^3, respectively. The effective frozen soil particle size affects the albedo and optical thickness of frozen soil. As shown in Fig. 11, the simulated Tb at C-, X-, Ku-bands, and Ka-band decreased as the effective frozen soil particle size increased. It is worth noting that the shorter the wavelength, the more pronounced is the tendency for Tb to decrease with increasing effective frozen soil particle size. The shorter the wavelength the greater the albedo, and optical thickness is with the same effective frozen soil particle size (Fig. 12). The albedo at C- to Ka-bands begins to change significantly after the effective frozen soil particle size reaches 0.35, 0.25, 0.1, and 0.05 cm, respectively. The optical thickness at C- to Ka-bands begins to change significantly after the effective frozen soil particle size reaches 0.7, 0.45, 0.25, and 0.1 cm, respectively. The changes in the simulation results with increasing effective frozen soil particle size were, however, barely noticeable in the L-band. The higher the frequency was, the more obviously the simulations were affected by the effective frozen soil particle size. This indicates that 1) volume scattering should be considered at Ku- and Ka-bands even if the effective frozen soil particle size is small; 2) the effect of volume scattering on C- and X-bands is related to the effective frozen soil particle size; and 3) the volume scattering effect could be ignored at L-band since the wavelength is much larger than the soil particle size.

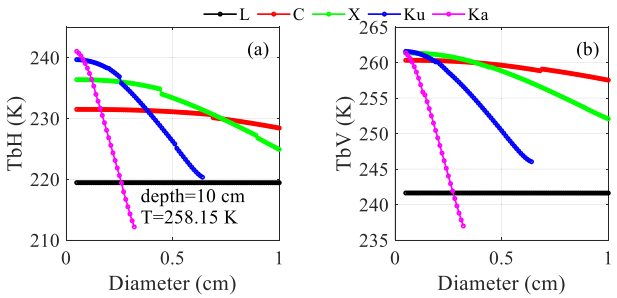

Fig. 11. Sensitivity of effective frozen soil particle size to Tb. (a) H-polarization and (b) V-polarization.

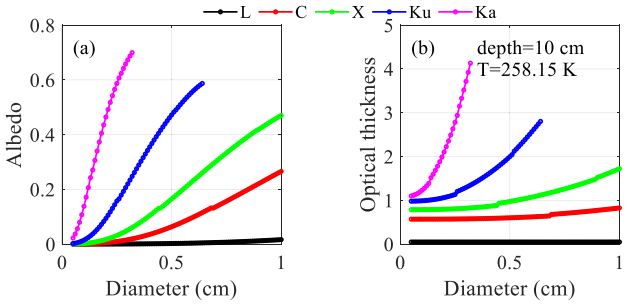

Fig. 12. Dependence of (a) albedo and (b) optical thickness on the effective frozen soil particle size.

D. Soil Frost Depth on Tb Simulation

The Tb from L- to Ka-band with soil frost depths ranging from 1 to 100 cm with a step size of 5 cm were simulated. The effective frozen soil particle size and soil moisture of the unfrozen soil layer were 0.1 cm and 0.15 m^3/m^3, respectively. The dielectric constants of the scatterers are the same as in the previous section. The sand content, clay content, and bulk density of the soil were 60%, 20%, and 1.3 g/cm^3, respectively. As shown in Fig. 13, the simulated Tb at L-band increased as the frost depth increased. The simulated Tb at H-polarization increased before the frost depth increased to 20, 15, 10, and 5 cm at C-, X-, Ku-, and Ka-bands, respectively, and then decreased with increasing frost depth. The simulated Tb at V-polarization increased before the frost depth increased to 15 and 5 cm at C- and X-bands, respectively, and then decreased with increasing frost depth. The simulated Tb at V-polarization decreased as the frost depth increased at Ku- and Ka-bands. Soil frost depth affected the optical thickness of frozen soil. The greater the soil frost depth was, the greater the optical thickness. The radiation of bottom unfrozen soil would be attenuated by frozen soil, and the radiation contribution of frozen soil would increase until the frost depth reaches the penetration depth of each band. Take H-polarization as an example, and the simulated Tb at C- to Ka-bands increases first with increasing frost depth because the lower emission from bottom unfrozen soil is being attenuated at this time, while the effect of higher frozen soil emission on simulated Tb is increasing. Once the frost depth increased to 20, 15, 10, and 5 cm at C-, X-, Ku-, and Ka-bands, respectively, it is possible these four bands can no longer penetrate the top frozen soil layer to receive the microwave emission from the bottom unfrozen soil and the downward-emitted frozen soil radiation scattered by unfrozen-frozen soil interface was attenuated by top frozen soil. Then, the extinction effect caused by volume

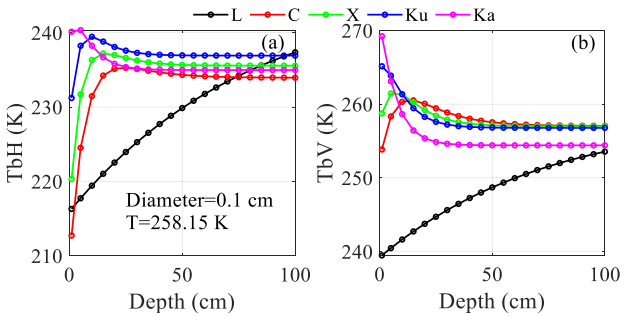

Fig. 13. Dependence of Tb on soil frost depth. (a) H-polarization and (b) V-polarization.

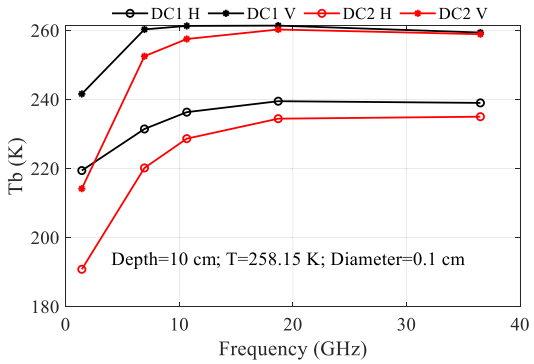

Fig. 14. Dependence of Tb on the dielectric constant of scatterers.

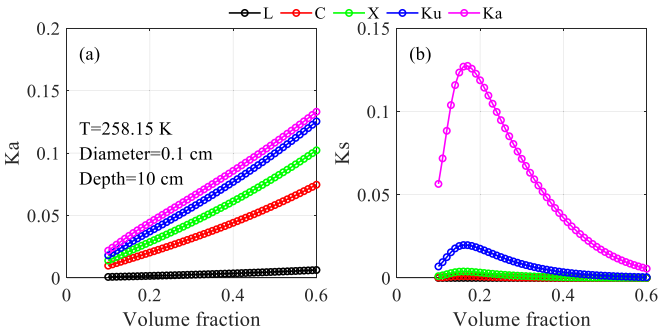

Fig. 15. Dependence of (a) absorption coefficient and (b) scattering coefficient on the fractional volume of scatterers.

scattering from frozen soil and the attenuation of the top frozen soil becomes the main factor affecting the passive microwave Tb; as the frost depth continues to increase, the optical thickness increases and the Tb decreases. The different performance of simulated Tb at H- and V-polarization with increasing frost depth may be due to the different penetration depths of V- and H-polarization into the permafrost. The simulated Tb at the L-band keeps increasing because the maximum frost depth simulated here has not yet reached the penetration depth of the L-band into frozen soil, and the L-band is not sensitive to volume scattering effects. The increase contribution of emission from frozen soil dominates the increase in the simulated Tb at L-band. The variation in simulated Tb with frost depth among L- to Ka-bands was different because the penetration depth varied across different frequencies.

E. Different Dielectric Constant of Scatterers on Tb Simulation

The dielectric constant of scatterers affected the effective dielectric constant, scattering coefficient, and absorption coefficient of frozen soil, etc., and may be different at the same band due to different soil moisture and soil texture (related to the amount of bound water adhering to the surface of soil minerals). To analyze the effect of the dielectric constant of scatterers on the Tb simulation using SFS_DMRT, Tb from L- to Ka-band with two different dielectric constants of scatterers cases: 1) 4.4 + 0.17i at L-band, 3.7 + 0.23i at C-band, 3.5 + 0.2 i at X-band, 3.2 + 0.13 i at Ku-band and 3.1 + 0.07 i at Ka-band, respectively, respectively (DC1) and 2) 4.8 + 0.15 i at L-band, 4.2 + 0.23 i at C-band, 3.9 + 0.2 i at X-band, 3.6 + 0.13 i at Ku-band and 3.5 + 0.07 i at Ka-band, respectively (DC2) were simulated. The soil frost depth was set to 10 cm. The sand content, clay content, and bulk density of the soil were 60%, 20%, and 1.3 g/cm^3, respectively. The effective dielectric constant of frozen soil with a large dielectric constant of scatterers was greater than that with a small dielectric constant of scatterers. Fig. 14 shows the dependence of Tb on the dielectric constant of scatterers. The smaller simulated Tb values were simulated with a larger dielectric constant of scatterers. The higher the frequency, the smaller the difference between the Tb obtained from the two dc cases. At low frequencies, where the volume scattering effect is insignificant, the simulated Tb is mainly affected by the dielectric constant of the medium. At high frequencies, the small simulated Tb difference is the result of a combination of dielectric constant and volume scattering effects.

Soil texture and bulk density also affected the Tb simulated by SFS_DMRT by influencing the fractional volume of scatterers in frozen soil. Fig. 15 shows the dependence of the absorption coefficient (Ka) and scattering coefficient (Ks) on the fractional volume of scatterers. From Fig. 15, it can be seen that Ka increases almost linearly with the fractional volume. Ks first increases and then decreases with the increase of fractional volume of scatterers. For low fractional volume, the medium is sparse, and the scattering coefficient increases with the increase of fractional volume. For fractional volumes larger than 0.15, the scatterers are considered to be nonindependent, which weakens their scattering efficiency [52].

V. Conclusion

In this study, a radiation transfer model (SFS_DMRT) for the seasonally frozen ground was developed to consider the volume scattering effects inside frozen soil based on DMRT and Mie spherical scattering theory. The soil was considered as a vertical heterostructure with a frozen layer at the top and an unfrozen layer at the bottom. The microwave emissions from the rough interfaces between unfrozen-frozen soil and frozen air were simulated with Qp models. Ground-based microwave radiometer data from three different experimental sites were used to validate the SFS_DMRT model. Results show that in Sodankylä, where the soil is in a stable frozen state, the Tb simulated by SFS_DMRT has a higher agreement with observed Tb versus AIEM. The effect of

volume scattering from a thin transition layer could narrow the polarization difference and improve the simulations at the snow-removed surface. The emission of frozen soil can, moreover, be described by AIEM without considering the volume scattering effect at the A'rou site, where the soil was undergoing diurnal F/T cycles. Also, results in Yudaokou show that the SFS_DMRT model is ineffective in simulating the passive microwave emissions of frozen soil with a negative temperature but close to 0 °C, where the soil was undergoing interday F/T cycles. The sensitivity of SFS_DMRT to frozen soil parameters was also analyzed. The effect of volume scattering could be ignored at the L-band, the degree of volume scattering at C- and X-bands depended on the effective frozen soil particle size, and the effect of volume scattering must be considered in Ku- and Ka-bands for frozen soil. The attenuation of emission from bottom unfrozen soil was determined by the soil frost depth and penetration depth of the microwave bands. The dielectric constant of scatterers, soil texture, soil bulk density, and soil temperature also affected the simulated Tb. It should be possible to ignore volume scattering at low frequencies (i.e., L- and C-band) and to consider single volume scattering or only consider surface scattering. Future applications of the SFS_DMRT model include retrieving soil frost depth and obtaining the stratified profile information of soil.

ACKNOWLEDGMENT

The authors would like to thank the Finnish Meteorological Institute for providing the ground-based microwave radiometric data from the Sodankylä experimental site.

REFERENCES

[1] J. S. Kimball, K. C. McDonald, S. Frolking, and S. W. Running, "Radar remote sensing of the spring thaw transition across a boreal landscape," *Remote Sens. Environ.*, vol. 89, no. 2, pp. 163–175, Jan. 2004.

[2] K. C. McDonald and J. S. Kimball, "Estimation of surface freeze-thaw states using microwave sensors," in *Encyclopedia of Hydrological Sciences*, M. G. Anderson, Eds., West Sussex, U.K.: Wiley, 2005, pp. 783–797.

[3] X. Zhang et al., "Time-series InSAR monitoring of permafrost freeze-thaw seasonal displacement over Qinghai–Tibetan Plateau using Sentinel-1 data," *Remote Sens.*, vol. 11, no. 9, p. 1000, Apr. 2019.

[4] P. Lu, J. Han, T. Hao, R. Li, and G. Qiao, "Seasonal deformation of permafrost in Wudaoliang basin in Qinghai–Tibet Plateau revealed by StaMPS-InSAR," *Mar. Geodesy*, vol. 43, no. 3, pp. 248–268, May 2020.

[5] J. Wang, C. Wang, H. Zhang, Y. Tang, X. Zhang, and Z. Zhang, "Small-baseline approach for monitoring the freezing and thawing deformation of permafrost on the Beiluhe basin, Tibetan Plateau using TerraSAR-X and Sentinel-1 data," *Sensors*, vol. 20, no. 16, p. 4464, Aug. 2020.

[6] Y. Kim, J. S. Kimball, J. Glassy, and J. Du, "An extended global Earth system data record on daily landscape freeze–thaw status determined from satellite passive microwave remote sensing," *Earth Syst. Sci. Data*, vol. 9, no. 1, pp. 133–147, Feb. 2017.

[7] C. Derksen et al., "Retrieving landscape freeze/thaw state from soil moisture active passive (SMAP) radar and radiometer measurements," *Remote Sens. Environ.*, vol. 194, pp. 48–62, Jun. 2017.

[8] P. Wang et al., "Parameterization of the freeze/thaw discriminant function algorithm using dense in-situ observation network data," *Int. J. Digit. Earth*, vol. 12, no. 8, pp. 980–994, Aug. 2019.

[9] V. Naeimi et al., "ASCAT surface state flag (SSF): Extracting information on surface freeze/thaw conditions from backscatter data using an empirical threshold-analysis algorithm," *IEEE Trans. Geosci. Remote Sens.*, vol. 50, no. 7, pp. 2566–2582, Jul. 2012.

[10] K. Rautiainen et al., "L-band radiometer observations of soil processes in boreal and subarctic environments," *IEEE Trans. Geosci. Remote Sens.*, vol. 50, no. 5, pp. 1483–1497, May 2012.

[11] K. Rautiainen et al., "Detection of soil freezing from L-band passive microwave observations," *Remote Sens. Environ.*, vol. 147, pp. 206–218, May 2014.

[12] N. Baghdadi, H. Bazzi, M. El Hajj, and M. Zribi, "Detection of frozen soil using Sentinel-1 SAR data," *Remote Sens.*, vol. 10, no. 8, p. 1182, Jul. 2018.

[13] A. Roy et al., "Response of L-band brightness temperatures to freeze/thaw and snow dynamics in a Prairie environment from ground-based radiometer measurements," *Remote Sens. Environ.*, vol. 191, pp. 67–80, Mar. 2017.

[14] Y. Kim, J. S. Kimball, K. C. McDonald, and J. Glassy, "Developing a global data record of daily landscape freeze/thaw status using satellite passive microwave remote sensing," *IEEE Trans. Geosci. Remote Sens.*, vol. 49, no. 3, pp. 949–960, Mar. 2011.

[15] B. W. Zuerndorfer, A. W. England, M. C. Dobson, and F. T. Ulaby, "Mapping freeze/thaw boundaries with SMMR data," *Agricult. Forest Meteorol.*, vol. 52, nos. 1–2, pp. 199–225, Aug. 1990.

[16] T. Zhang, R. L. Armstrong, and J. Smith, "Investigation of the near-surface soil freeze-thaw cycle in the contiguous United States: Algorithm development and validation," *J. Geophys. Res., Atmos.*, vol. 108, no. D22, p. 8860, Nov. 2003.

[17] B. Zuerndorfer and A. W. England, "Radiobrightness decision criteria for freeze/thaw boundaries," *IEEE Trans. Geosci. Remote Sens.*, vol. 30, no. 1, pp. 89–102, Jan. 1992.

[18] J. Wang et al., "Evaluation and analysis of SMAP, AMSR2 and MEaSUREs freeze/thaw products in China," *Remote Sens. Environ.*, vol. 242, Jun. 2020, Art. no. 111734.

[19] J. Johnston, V. Maggioni, and P. Houser, "Comparing global passive microwave freeze/thaw records: Investigating differences between Ka- and L-band products," *Remote Sens. Environ.*, vol. 247, Sep. 2020, Art. no. 111936.

[20] D. Zheng et al., "L-band microwave emission of soil freeze–thaw process in the third pole environment," *IEEE Trans. Geosci. Remote Sens.*, vol. 55, no. 9, pp. 5324–5338, Sep. 2017.

[21] T. L. Rowlandson et al., "Capturing agricultural soil freeze/thaw state through remote sensing and ground observations: A soil freeze/thaw validation campaign," *Remote Sens. Environ.*, vol. 211, pp. 59–70, Jun. 2018.

[22] D. Zheng et al., "Sampling depth of L-band radiometer measurements of soil moisture and freeze-thaw dynamics on the Tibetan Plateau," *Remote Sens. Environ.*, vol. 226, pp. 16–25, Jun. 2019.

[23] D. Zheng et al., "Impact of soil permittivity and temperature profile on L-band microwave emission of frozen soil," *IEEE Trans. Geosci. Remote Sens.*, vol. 59, no. 5, pp. 4080–4093, May 2021.

[24] M. Schwank, M. Stahli, H. Wydler, J. Leuenberger, C. Matzler, and H. Fluhler, "Microwave L-band emission of freezing soil," *IEEE Trans. Geosci. Remote Sens.*, vol. 42, no. 6, pp. 1252–1261, Jun. 2004.

[25] T. Zhao, L. Zhang, L. Jiang, S. Zhao, L. Chai, and R. Jin, "A new soil freeze/thaw discriminant algorithm using AMSR-E passive microwave imagery," *Hydrol. Processes*, vol. 25, no. 11, pp. 1704–1716, May 2011.

[26] A. W. England, J. F. Galantowicz, and B. W. Zuerndorfer, "A volume scattering explanation for the negative spectral gradient of frozen soil," in *Proc. IGARSS Remote Sens., Global Monit. Earth Manage.*, vol. 3, Jun. 1991, pp. 1175–1177.

[27] H. Lu et al., "A radiative transfer model for soil media with considering the volume effects of soil particles: Field observation and numerical simulation," in *Proc. IEEE Int. Symp. Geosci. Remote Sens.*, Aug. 2006, pp. 1736–1739.

[28] C. Onier, A. Chanzy, A. Chambarel, R. Rouveure, M. Chanet, and H. Bolvin, "Impact of soil structure on microwave volume scattering evaluated by a two-dimensional numerical model," *IEEE Trans. Geosci. Remote Sens.*, vol. 49, no. 1, pp. 415–425, Jan. 2011.

[29] J. Du, J. Kimball, and M. Moghaddam, "Theoretical modeling and analysis of L- and P-band radar backscatter sensitivity to soil active layer dielectric variations," *Remote Sens.*, vol. 7, no. 7, pp. 9450–9472, Jul. 2015.

[30] Z. Hao, S. Zhao, L. Zhang, L. Jiang, and L. Xiao, "Comparison of microwave emission model for frozen soil and field observation," in *Proc. IEEE Int. Geosci. Remote Sens. Symp.*, New York, NY, USA, Jul. 2011, pp. 3097–3100.

[31] A. Fung, *Microwave Scattering and Emission Models and Their Applications*. Boston, MA, USA: Artech House, Jan. 1994.

[32] J. Wang, L. Jiang, X. Liu, and J. Yang, "Development of microwave emission model for frozen soil with considering the volume scattering effect," in *Proc. IEEE Int. Geosci. Remote Sens. Symp.*, Sep. 2020, pp. 3078–3081.

[33] L. Jiang, J. Shi, S. Tjuatja, J. Dozier, K. Chen, and L. Zhang, "A parameterized multiple-scattering model for microwave emission from dry snow," *Remote Sens. Environ.*, vol. 111, nos. 2–3, pp. 357–366, Nov. 2007.

[34] M. Shao, Q. Wang, and M. Huang, *Soil Physics*. Beijing, China: Higher Education Press, 2006.

[35] D. Liang, X. Xu, L. Tsang, K. M. Andreadis, and E. G. Josberger, "The effects of layers in dry snow on its passive microwave emissions using dense media radiative transfer theory based on the quasicrystalline approximation (QCA/DMRT)," *IEEE Trans. Geosci. Remote Sens.*, vol. 46, no. 11, pp. 3663–3671, Nov. 2008.

[36] J. Shi, L. Jiang, L. Zhang, K.-S. Chen, J.-P. Wigneron, and A. Chanzy, "A parameterized multifrequency-polarization surface emission model," *IEEE Trans. Geosci. Remote Sens.*, vol. 43, no. 12, pp. 2831–2841, Dec. 2005.

[37] T. Zhao et al., "Multi-frequency microwave radiometric measurements of soil freeze-thaw process over seasonally frozen ground," in *Proc. IEEE Int. Geosci. Remote Sens. Symp. (IGARSS)*, Jul. 2017, pp. 4258–4261.

[38] J. Lemmetyinen et al., "Retrieval of effective correlation length and snow water equivalent from radar and passive microwave measurements," *Remote Sens.*, vol. 10, no. 2, p. 170, Jan. 2018.

[39] S. Feng et al., "Miscellaneous methods for determination of unfrozen water content in frozen soils," *J. Hydrol.*, vol. 631, Mar. 2024, Art. no. 130802.

[40] Q. Cheng et al., "In situ measured and simulated seasonal freeze–thaw cycle: A 2-year comparative study between layered and homogeneous field soil profiles," *J. Hydrol.*, vol. 519, pp. 1466–1473, Nov. 2014.

[41] A. K. Fung, K.-S. Chen, and K. Chen, *Microwave Scattering and Emission Models for Users*. Norwood, MA, USA: Artech House, 2010.

[42] L. Tsang, J. Pan, D. Liang, Z. Li, D. W. Cline, and Y. Tan, "Modeling active microwave remote sensing of snow using dense media radiative transfer (DMRT) theory with multiple-scattering effects," *IEEE Trans. Geosci. Remote Sens.*, vol. 45, no. 4, pp. 990–1004, Apr. 2007.

[43] L. Tsang, A. K. Jin, and R. T. Shin, *Theory of Microwave Remote Sensing*. New York, NY, USA: Wiley, 1985.

[44] S. Pettinato, E. Santi, M. Brogioni, S. Paloscia, E. Palchetti, and C. Xiong, "The potential of COSMO-SkyMed SAR images in monitoring snow cover characteristics," *IEEE Geosci. Remote Sens. Lett.*, vol. 10, no. 1, pp. 9–13, Jan. 2013.

[45] E. Santi et al., "Analysis of microwave emission and related indices over snow using experimental data and a multilayer electromagnetic model," *IEEE Trans. Geosci. Remote Sens.*, vol. 55, no. 4, pp. 2097–2110, Apr. 2017.

[46] M. Brogioni and P. Pampaloni, "A theoretical analysis on the sensitivity of microwave emission to snow parameters," in *Proc. Microw. Radiometry Remote Sens. Environ.*, Florence, Italy, 2008, pp. 1–4.

[47] J. R. Wang, P. E. O'Neill, T. J. Jackson, and E. T. Engman, "Multifrequency measurements of the effects of soil moisture, soil texture, and surface roughness," *IEEE Trans. Geosci. Remote Sens.*, vol. GE-21, no. 1, pp. 44–51, Jan. 1983.

[48] N. Jiang, H. Li, Y. Liu, H. Li, and D. Wen, "Pore microstructure and mechanical behaviour of frozen soils subjected to variable temperature," *Cold Regions Sci. Technol.*, vol. 206, Feb. 2023, Art. no. 103740.

[49] D. Liang, L. Tsang, S. Yueh, and X. Xu, "Modeling active microwave remote sensing of multilayer dry snow using dense media radiative transfer theory," in *Proc. IEEE Int. Geosci. Remote Sens. Symp.*, vol. 3, Jul. 2008, pp. III-39–III-42.

[50] L. Jiang, S. Tjuatja, J. Shi, L. Zhang, and K. Zhao, "Evaluation of emission from snow-covered ground for passive microwave remote sensing," *Int. J. Remote Sens.*, vol. 33, no. 3, pp. 872–886, Feb. 2012.

[51] L. Tsang, C.-T. Chen, A. T. C. Chang, J. Guo, and K.-H. Ding, "Dense media radiative transfer theory based on quasicrystalline approximation with applications to passive microwave remote sensing of snow," *Radio Sci.*, vol. 35, no. 3, pp. 731–749, May 2000.

[52] D. Liang, K. Tse, Y. Tan, L. Tsang, and K. H. Ding, "Scattering and emission in snow based on QCA/DMRT and numerical Maxwell model of 3Dimentional simulations (NMM3D)," in *Proc. IEEE MicroRad*, Mar. 2006, pp. 197–202.

Jian Wang received the B.S. degree from Yanshan University, Qinhuangdao, China, in 2016, and the Ph.D. degree in cartography and geography information systems from Beijing Normal University, Beijing, China, in 2023.

She is currently an Assistant Professor with the Institute of Forest Resource Information Techniques, Chinese Academy of Forestry, Beijing. Her research interests include microwave emission/scattering modeling of soil, and microwave remote sensing of land surface freeze/thaw state and forest parameter inversion.

Lingmei Jiang (Member, IEEE) received the Ph.D. degree in geography from Beijing Normal University, Beijing, China, in July 2005.

She is a Professor with the Faculty of Geographical Science, Beijing Normal University. She has authored/co-authored over 200 scientific publications. Her research interests include microwave emission/scattering modeling of the land surface, passive microwave remote sensing of snow water equivalent and soil moisture, surface freeze/thaw state, and remote sensing data assimilated into the land surface model.

Dr. Jiang has received the Shi Yafeng Award for Young Scientists in Cryosphere and Environment in 2018, and Li Xiaowen Remote Sensing Science Award in 2023.

Tianjie Zhao (Senior Member, IEEE) received the B.S. and Ph.D. degrees from Beijing Normal University, Beijing, China, in 2007 and 2012, respectively.

From 2010 to 2012, he was a Visiting Scientist with the Hydrology and Remote Sensing Laboratory, Agricultural Research Service (ARS), U.S. Department of Agriculture, Beltsville, MD, USA. He is currently a Research Professor with the State Key Laboratory of Remote Sensing Science, Aerospace Information Research Institute, Chinese Academy of Sciences (CAS), Beijing. His research interests include microwave remote sensing of soil moisture and its freeze-thaw process.

Dr. Zhao was a recipient of the scholarship award for excellent doctoral student granted by the Ministry of Education of China in 2011, the Young Scientist Award from the International Union of Radio Science (URSI) in 2014, the Young Scientist Award from Progress in Electromagnetics Research Symposium (PIERS) in 2018, and the Li Xiaowen Youth Award in Remote Sensing Science in 2023.

Huizhen Cui (Member, IEEE) received the Ph.D. degree in cartography and geographic information systems from the Faculty of Geographical Science, Beijing Normal University, Beijing, China, in July, 2019.

From 2017 to 2018, she was a Visiting Ph.D. Student with the Institute of Applied Physics, National Research Council (IFAC-CNR), Florence, Italy. She is currently a Research Assistant with National Space Science Center, Chinese Academy of Sciences, Beijing. Her research interests include the microwave remote sensing of soil moisture and microwave emission and scattering modeling of land surface.

Yinghong Luan received the Ph.D. degree from Nanjing University of Science and Technology, Nanjing, China, in 2010.

She is currently an Engineer of Shanghai Academy of Spaceflight Technology, Shanghai, China. Her research interests include microwave remote sensing, payload for soil moisture detection design, and spacecraft design.